# PREDICTING FAILURE MECHANISMS IN T-SHAPED AEROSPACE COMPOSITE STRUCTURES

F. Hélénon[1], M.R. Wisnom[1], S.R. Hallett[1*] and R.S. Trask[1]
[1] Advanced Composites Centre for Innovation and Science, University of Bristol, Queen's Building, University Walk, Bristol BS8 1TR, UK
* Corresponding author (fabrice.helenon@bristol.ac.uk)

**Keywords**: *Composite Structures, Stress Concentration, Delamination, Failure Initiation*

## 1. General introduction

This work addresses the problem of modelling via commercially available finite element (FE) codes the failure mechanisms in laminated composite joints such as T-shaped specimens, which are typically encountered in vanes, stiffeners and other aerospace structures. Because of their relative complexity, the prediction of both their damage resistance and failure mechanism is fundamental for a conservative design. In this paper, experimental and numerical investigations are presented on specimens manufactured from IM7/8552 carbon/epoxy pre-impregnated laminates.

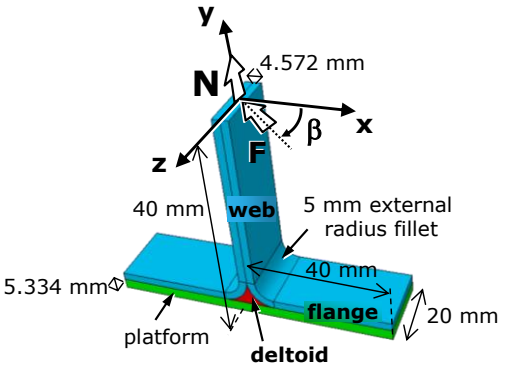


Fig. 1: Details of the loading direction (**N**: tension pull-off; **F**: bending force at an angle β).

Four load-to-failure cases are undertaken; see fig. 1: one pull-off tension and three out-of-plane bending cases at angles β = 0º, 45º and 90°. 3D linear elastic FE analyses are performed and discussed. The stress field is interpreted with the maximum principal stress defined in the plane perpendicular to the fibre direction. The High Stress Concentration (HSC) method [3] is subsequently used to assess the free-edge stresses and to predict the specimen's failure load. It consists of comparing, in the close neighbourhood of a stress concentration, any FE stress distribution with the distribution induced by the presence of an abstract crack on the point of propagating. If the stress levels encountered in the FE analysis are less than what could be induced by this abstracted crack, they should be without any consequences on the composite structure. The predictions are then confirmed via non-linear FE analyses involving interface elements.

## 2. Experimental results

The T-piece specimen under consideration in this paper, see fig. 1, is composed of three separately laid-up sections: two curved and one straight with a fill-in deltoid region made from 90º unidirectional tows of the same material system. The flange has a $(60/0/\text{-}60/0)_{3S}$ layup for the platform plus a $(\pm 45_2/0_7/90_4/0_3)$ lay-up which has come down from the web. More experimental and manufacturing details can be found in [5]. The experimental testing configurations for specimens with the deltoid areas corresponding to the nominal dimensions and the enlarged pictures at failure of the crack formation are given in figs. 2-5. Table 1 summarises the average failure load values obtained from the four test cases.

| Tension | Bending β = 0° | Bending β = 45° | Bending β = 90° |
|---|---|---|---|
| 1330 N (9 %) | 385 N (10.2 %) | 522 N (3.2 %) | 898 N (6.4 %) |

Table 1: Average failure loads from testing. The percentages indicate the coefficients of variation.

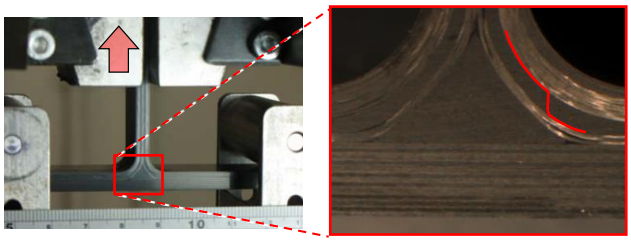

Fig. 2: Pull-off tension: For some test cases, cracks initiated in the curved region of the $90_4$ block, then propagated along the $90_4/0_7$ and $0_3/90_4$ interfaces; for other test cases, cracks initiated at the deltoid/$0_3$ interface then propagated through the deltoid down to the platform region [2].

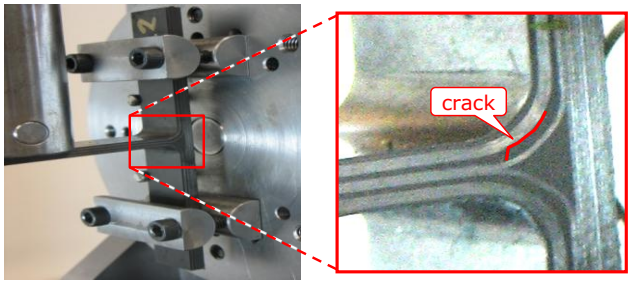


Fig. 3: Bending at β = 0°: Crack initiating at the same location as in fig 2 but further up, then propagating along the $90_4/0_7$ interface.

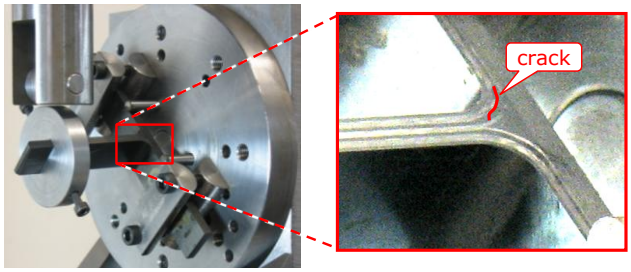


Fig. 4: Bending at β = 45°: Similar mechanism as in fig 3 but with a crack initiating slightly further down in the fillet.

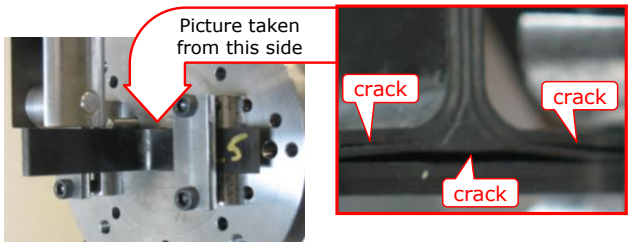


Fig. 5: Bending at β = 90°: Cracks initiating in the left and right $90_4$ blocks just above the lower deltoid tips. Next, crack occurring at the platform/deltoid interface.

## 3. Damage onset and crack pattern prediction

### 3.1. Preliminary linear elastic FE analyses

3D FE analyses are first performed for each load case by using two distinct steps. The first aims to model the cure phase (ΔT = -160 °C) and the second focuses on subsequent mechanical stresses generated when applying the average failure load measured experimentally (see table 1) in addition to the residual stresses. Fig 6 gives an overview of the FE mesh employed. Globally, one quadratic element is introduced per 0.127 mm thick ply. A higher in plane density of elements is introduced at the free-edges in order to guarantee a satisfactory capture of the stress gradients. Across the width, 10 elements 0.2 mm wide are used at the free-edge region then 12 elements with sizes starting from 0.233 to 1.4 mm at the vertical middle plane of symmetry are used. The boundary conditions, see fig. 1, are modified according the load case. For the pull-off tension case, only a quarter-geometry is used as discussed in [2]. Symmetry boundary conditions are therefore employed where necessary. The support (roller in fig. 2) is modelled by preventing all the nodes on a line across the top surface of the flange from moving vertically. The top of the web is loaded with a uniform tensile stress distribution consistent with the average failure load **N**. Regarding the out-of-plane bending cases, the ends of the platform are clamped to model the presence of the "half-moon" supports firmly screwed together; see figs. 3-5. The top end surface of the web, being at 60 mm from the underside of the flange, is subjected to a uniform shear stress consistent with the applied lateral failure load **F**.

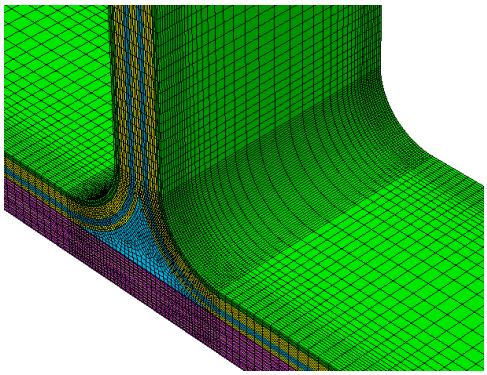

Fig. 6: Isometric view of the FE mesh used (mesh B).

Careful post-processing analysis of all the FE results shows that several stress tensor components are very high, particularly those within the 1-2-plane of both of the $90_4$ blocks and the deltoid region shown in fig. 7. Because of the complexity in interpreting the results, it is chosen to plot the maximum principal stress component defined in the plane perpendicular to the fibre direction. This shows that both the deltoid region and the $90_4$ blocks are the most sensitive regions irrespective of the load case. Indeed, high free-edge HSCs are observed at those locations, see example in fig. 7. Those values are found to be far above the 111 MPa material transverse tensile strength value [4].

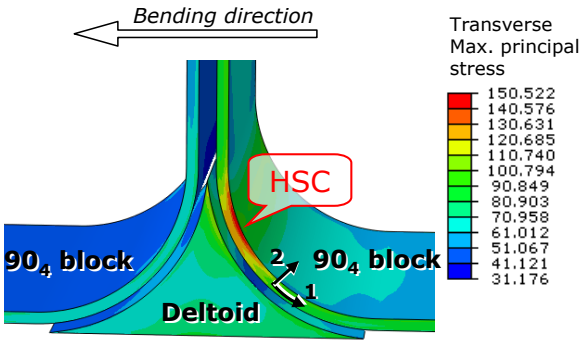


Fig. 7: Example of HSC phenomenon at the free-edge of the T-piece specimen for the bending case at $\beta = 0^o$. For simplicity, only the $90_4$ blocks and deltoid region are shown.

A further investigation into the principal direction associated with the chosen maximum principal stress component reveals that, for each of the four load cases, both the location of failure initiation and the original crack propagation direction are in good agreement with the experimental observations summarised in section 2. However, because the HSCs are highly localised at the free-edge, it is not possible to conclude if they will lead to failure. Their distributions have to be compared with those induced by the presence of abstracted cracks on the point of propagating from the same locations as per the previously presented HSC method [3].

### 3.2. Post-processing of the FE results with the HSC method

To be able to conclude about the criticality of the high-localised free-edge stresses, the HSC method is employed [3]. By selecting, for each load case, the most loaded node within the FE mesh and relevant interlaminar crack paths, it is possible to assess the criticality of the HSCs. Fig. 8 shows an example of application to the $0^o$ bending case, i.e. the graph plotting the stress distribution (FE curve) across the width from the free-edge of the $90_4$ block. This curve is compared to the material transverse tensile strength line, $\sigma_{Max}$ = 111 MPa, and the critical curve, $\sigma_c$, giving the theoretical stress field ahead of a crack on the point of propagating.

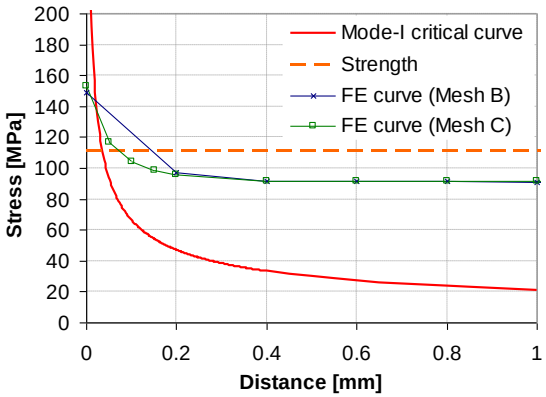


Fig. 8: Example of application of the HSC method to the $90_4$ block for the $0^o$ bending case at the experimental failure load **F** = 385 N.

In this example, two FE curves are plotted in order to assess the influence of the mesh refinement. Mesh C is a sub-model in the region of HSC similar to mesh B but with 4 rows of elements 0.05 mm wide at the free-edge instead of one row. Since the FE curve crosses the critical curve above $\sigma_{Max}$, therefore failure is confirmed for the load **F** = 385 N used in the FE model. Similar assessments have been also made with the HSC method for the pull-off tension as well as for the bending cases at $45^o$ and $90^o$. They have all confirmed failure because all the FE curves crossed the critical curve above the material strength line.

### 3.3. Predictive investigation

The capability of the HSC method to assess failure is now extended to predicting failure load rather than just an assessment of the criticality of HSCs at given loads. When increasing the applied load, failure is expected to occur if the FE stress distribution, the

material strength line and the critical curve cross together at the same point, see fig, 9. Using this criterion it is possible to predict failure loads for the various cases and meshes examined as summarised in table 2.

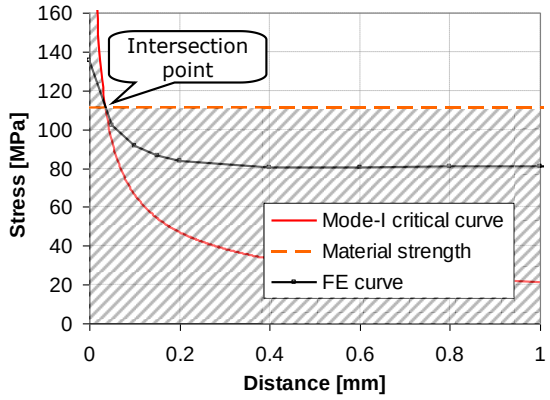


Fig. 9: Criterion used for predicting the failure load with the HSC method. The hatched region is the safe zone.

| | Tension | Bending β = 0° | Bending β = 45° | Bending β = 90° |
|---|---|---|---|---|
| Mesh B | 1030 (-22.6%) | 245 (-36%) | 275 (-47%) | 520 (-42%) |
| Mesh C | 1270 (-4.5%) | 305 (-21%) | 340 (-35%) | 620 (-31%) |

Table 2: Predicted failure loads (in N) by using the HSC method. The percentages indicate the difference compared with the experimental values given in table 1.

The predictions with Mesh B are very conservative but do provide a means to assess HSCs which cannot otherwise be dealt with by stress based failure criteria. The finer the mesh (mesh C compared with mesh B), the better the agreement with the experimental data in table 1. This is better than the usual situation where mesh refinement typically leads to less conservative results. To improve the accuracy of the simulation it is necessary to further investigate the phenomena occurring during physical testing, such as the effect of moisture.

### 3.4. Predictions by accounting for effect of moisture

As seen above, the failure mechanism of the T-piece specimen is free-edge dominated. Since the high free edge stresses are extremely localised, moisture can easily be absorbed in these regions, which will tend to release the edge residual stresses. In order to account for this effect it is proposed to simply consider the effect of a 2D uniform residual stress distribution across the width from the mid-plane of symmetry up to the free-edges. This is appropriate since the overall residual stress distribution is quasi-uniform across the specimen width, and relaxation of stresses away from the free edge would take a considerable time. After applying the same criterion detailed in fig 9, the failure load values of the T-pieces in out-of-plane bending become closer to the experimental data; see table 3. Most of the results remain conservative, apart from the one with mesh C (+6.5%), although this case has a high coefficient of variation of 10.2% as reported in table 1. The pull-off tension test case has not been considered in this study due to the inconsistency in the crack locations observed experimentally. The latter is thought to be due to the internal voidage in the large deltoid region interacting with the crack at the specimen's failure [5]. The predicted crack locations for all the bending cases were all very close to the experimental observations.

| | Bending β = 0° | Bending β = 45° | Bending β = 90° |
|---|---|---|---|
| Mesh B | 305 (-21%) | 340 (-35%) | 620 (-31%) |
| Mesh C | 410 (+6.5%) | 465 (-11%) | 810 (-10%) |

Table 3: Predicted failure loads (in N) by using the HSC method accounting for a constant residual stress distribution (moisture effect). The percentages indicate the difference compared to the experimental values given in table 1.

### 3.5. Validation by using interface elements

Non-linear FE analyses involving interface elements are finally considered to confirm the predicted crack pattern. For simplicity, the specimen in pull-off tension is considered because it makes it possible to

use only a quarter-geometry, which significantly reduces the computation costs. The mesh given in fig 6 is re-used but converted into a FE model having linear elements only. The quality of the mesh refinement with regards to the numerical cohesive zone length [1] has been checked and was found to be appropriate for modelling stable crack propagation. Two different crack patterns, mesh B1 and mesh B2, meshed with interface elements have been tested, see fig 10. The transverse crack in fig. 10(b) was introduced where an HSC was observed on the linear elastic FE model, and its orientation was defined according to the direction of the maximum principal stress perpendicular to the fibre direction. More details about this work can be found in [2].

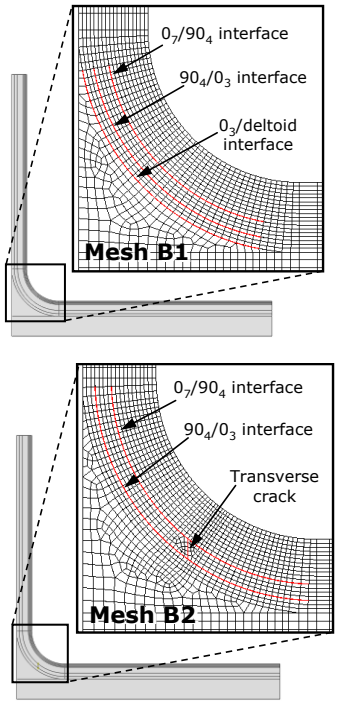


(a)

(b)

Fig. 10: Overview of the FE meshes from the lateral side with predefined crack paths: (a) Mesh B1 with interlaminar crack paths only. (b) Mesh B2 with interlaminar predefined crack path and with a transverse crack within the $90_4$ block.

A good agreement was found with the experimental failure mode captured in fig. 2 and the experimental average failure load of 1330 N. In addition, it has been found that the T-piece specimen failed suddenly due to propagation of the delamination and not due to the first onset of damage. This was possible because reduced maximum cohesive strength values were used to enable early failure initiation.

## 4. Conclusion

The HSC method was found to be a very efficient tool for predicting failure in T-shaped aerospace structures when using simple linear elastic FE analyses. By using this method in conjunction with the maximum principal stress defined perpendicularly to the fibre direction, both the crack initiation location and the original direction of the crack propagation can be predicted. This has been validated via the use of non-linear FE analyses involving interface elements.

## 4. Acknowledgements

The authors would like to acknowledge Rolls-Royce plc for their support of this research.

## 5. References

[1] P.W. Harper and S.R. Hallett. Cohesive zone length in numerical simulations of composite delamination. *Engineering Fracture Mechanics*, Vol. 75, No. 16, pp. 4774-4792, 2008.

[2] F. Hélénon, M.R. Wisnom, S.R. Hallett and R.S. Trask. "Numerical investigation into failure of laminated composite T-piece specimens under tensile loading". *Composites Part A* (submitted)

[3] F. Hélénon, M.R. Wisnom, S.R. Hallett and G. Allegri. "A method for dealing with high local stresses in finite element analyses". *Composites Part A*, Vol. 41, No. 9, pp 1156-1163, 2010.

[4] J. Lee and C. Soutis. Measuring the notched compressive strength of composite laminates: specimen size effects. *Composite Science and Technology*, Vol. 68, No. 12, pp 2359-2366, 2008.

[5] R.S. Trask, S.R. Hallett, F. Hélénon and M.R. Wisnom. "Influence of process induced defects on the failure of composite T-joint specimens". (to be submitted)